JOURNAL OF SPACECRAFT AND ROCKETS
Vol. 46, No. 2, March–April 2009

Experimental Verification of Heat-Flux Mitigation by Electromagnetic Fields in Partially-Ionized-Argon Flows

Ali Gülhan,* Burkard Esser,† Uwe Koch,† Frank Siebe,† and Johannes Riehmer†
DLR, German Aerospace Center, 51147 Cologne, Germany
Domenico Giordano‡
European Space Research and Technology Center, 2201 AZ Noordwijk, The Netherlands
and
Detlev Konigorski§
EADS Astrium, 28361 Bremen, Germany

DOI: 10.2514/1.39256

This paper describes an experimental study on heat-flux mitigation within high-enthalpy ionized-argon flows by application of an external magnetic-induction field. Two different axially symmetric test models containing water-cooled magnet coils have been investigated. The models have been made of a material with low thermal conductivity to visualize surface-temperature distribution. The latter has been measured by infrared thermography. Heat-flux rates have been derived from measured front- and rear-surface temperatures, taking into account temperature-dependent material characteristics and considering radiative-cooling exchange to the environment. Flowfield properties have been quantitatively characterized by laser-induced fluorescence, microwave interferometry, emission spectroscopy, electrostatic probes, and pitot probes. In addition, high-quality video recordings and photographs have been taken for shock-layer visualization. Remarkable measured surface-temperature reductions (16 and 44%) and derived heat-flux mitigations (46 and 85%) have been observed in the presence of an externally applied magnetic-induction field.

Nomenclature

B	=	magnetic field strength, T
D	=	diameter of the cylindrical model, mm
M	=	Mach number
m	=	mass, kg
N	=	number density, m^{-3}
q_c	=	conductive heat flux
q_r	=	radiative heat flux
q_t	=	convective heat flux, total heat flux,
Re	=	unit Reynolds number, m^{-1}
T	=	static temperature, K
t	=	time, s
v	=	flow velocity, $m \cdot s^{-1}$
x, r	=	axial, radial coordinate
λ	=	wave length, nm

Subscripts

ref	=	reference
W	=	wall
0	=	stagnation condition
1	=	freestream

Received 21 June 2008; revision received 5 September 2008; accepted for publication 18 September 2008.

*Head of the Windtunnel Department, Institute of Aerodynamic and Flow Technology, Linder Hoehe; Ali.Guelhan@dlr.de.
†Research Scientist, Windtunnel Department, Institute of Aerodynamic and Flow Technology, Linder Hoehe.
‡Research Engineer, Aerothermodynamics Section, Keplerlaan 1; Domenico.Giordano@esa.int. Member AIAA.
§Staff Engineer, P.O. Box 286156; Detlev.Konigorski@astrium.eads.net. Member AIAA.

I. Introduction

IN NOVEMBER 1957, Resler and Sears [1] submitted a seminal paper to the *Journal of the Aeronautical Sciences* in which they prospected the possibility of using electromagnetic fields for the purpose of controlling aerodynamic flows. Among several controllable effects, they mentioned heat-transfer reduction in boundary layers; this is an occurrence that is particularly appealing to aerothermodynamicists dealing with spacecraft thermal protection during planetary-atmosphere (re)entry. Their analysis, although based on rather crude physics and oversimplified flow-governing equations, led them to conclude that the subject matter was worthy of in-depth study, in view of the potential benefits for aeronautical and aerospace applications. One year later, they complemented [1] with a correction [2], which strengthened their conclusions, and Sears [3] replicated the positive message in another paper in 1959. Resler and Sears' [1] seminal paper, which appeared in April 1958, expectedly spawned strong interest among researchers in the scientific and engineering circles involved with magnetoaerodynamics and gave impetus to computational investigations of ionized super- and hypersonic flowfields in the presence of electromagnetic fields. In turn, the proliferation of computational investigations immediately made evident the necessity of well-designed and cleanly performed experiments, the findings of which could serve the important task of flow-solver validation. Indeed, shortly after the appearance of [1], Ziemer and Bush [4] computationally and experimentally investigated the influence of an externally applied magnetic-induction field on the shock standoff distance in ionized air flowing at $M = 4.5$ past a hemispherical cylinder in a shock tube. In September 1959, Ziemer [5] published a detailed description of the experiment. It turned out that when the pulsed electric current in the coaxial coils inside the cylinder produced an external magnetic induction of 4 T in the vicinity of the stagnation point, the shock-wave standoff distance increased by a factor of 7.5 with respect to the situation without magnetic induction. The effect was photographed and shown in both Fig. 1 of [4] and Fig. 9 of [5]; the photographs leave no doubt that there is a drastic influence of an externally applied magnetic-induction field on ionized flows. This conclusion can be

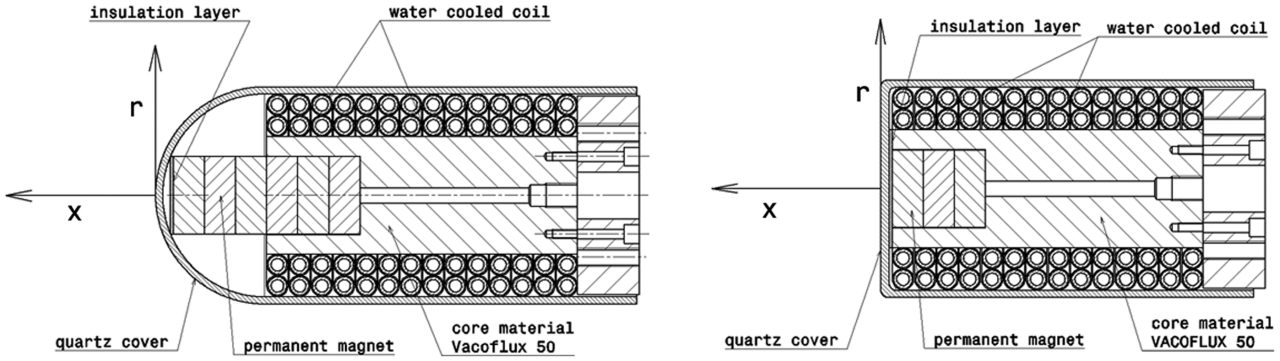

Fig. 1 Cross section view of the C2 (left) and C3 (right) model configurations.

considered to be experimentally proven knowledge, established since 1959.

The increase in shock-layer volume evidenced in Ziemer's [5] flowfield photographs suggested a relief of the heat-flux distribution on the hemispherical-cylinder wall, yet Ziemer did not attempt to measure the heat flux. In the early 1960s, Wilkinson [6] recognized that, notwithstanding considerable amount of computational work, very little experimental work had been done[¶] with the purpose in mind of measuring the heat-transfer reduction in ionized flows in the presence of electromagnetic fields, and he reported the findings of his own experiment. Wilkinson investigated the influence of an externally applied magnetic-induction field on the heat flux in the stagnation point of a blunt cone in ionized argon flowing at $M = 3$ from the supersonic nozzle of an arc jet. The experimental setup is shown in Figs. 1–3 of [6]; the adoption of permanent magnets (the model itself and another pole around the nozzle) to augment the externally applied magnetic induction required the positioning of the model very close to the nozzle exit. The measurement technique consisted of monitoring the time history of the stagnation-point temperature and then deriving the heat flux on the basis of the thin-wall model. The results, although somewhat scattered, indicated a monotonous decrease of the stagnation-point heat flux, down to almost 30%, with increasing magnetic-induction (squared) intensity (polarity north in Fig. 8 of [6]). Wilkinson's paper is rather instructive. He investigated the influence of the magnetic-induction polarity on the flowfield, remarked on the inadequacy of short-duration facilities for heat-flux measurements in the presence of electromagnetic fields, indicated the shortcomings of thermocouples in electromagnetic environments due to the appearance of stray electromotive forces that falsify temperature readings (page 428 of [6]), emphasized the importance of the tensorial nature of transport properties, unambiguously illustrated the inadequacy of the magnetic interaction parameter as a similitude parameter (Figs. 9 and 10 in [6]), and brought to light the weaknesses of computational models (Fig. 11 in [6]) that were being proposed in those years.

In the second half of the 1960s, Cambel et al. [7] and Kranc et al. [8] carried out an experimental program in magnetoaerodynamics that included heat-transfer investigations. In a progress report [7] to NASA, they provided preliminary information related to heat-flux measurements but did not release any quantitative data. They indicated that the tests were supposed to be performed in ionized argon flowing past a hemispherical cylinder with a magnetic-induction level of 0.3 T and that arrays of thermocouples were being used for temperature measurements and, in so doing, ignored Wilkinson's [6] experience mentioned earlier. Another report [8] from the same research team followed in 1969, but there was no mention of heat-transfer investigations. Finally, in November 1973, Nowak and Yuen [9] published a detailed description of a series of tests with ionized argon flowing at $M = 4.6$ past a hemispherical cylinder. They adopted the same measurement technique of Wilkinson [6]: temperature–time histories were recorded, by thermocouples in this case, and heat-flux distributions were derived via a transient thin-skin model. Measurements were carried out for both electrically conducting and nonconducting bodies (manufactured in copper and coated with Teflon as required), with and without an externally applied magnetic-induction field. Nowak and Yuen [9] found an unexpected result: the stagnation-point heat flux increased when the externally applied magnetic induction was present (Fig. 3 of [9]). Not only did the increase turn out to be as great as 60% in correspondence to a magnetic induction of 0.5 T for the electrically conducting body, but even for the electrically nonconducting body a slight increase was measured in correspondence to a magnetic induction of 0.32 T. Nowak and Yuen also found that in the situation without externally applied magnetic induction but with an electrically conducting body, Lees's [10] and Fay and Riddell's [11] empirical formulas became inadequate because they were unable to predict the increase in heat-flux distribution due to the electric currents entering the body (Fig. 1 of [9]). In light of Wilkinson's [6] experimentally substantiated counterargument about the use of thermocouples in electromagnetic environments, one may wonder how reliable Nowak and Yuen's [9] results can be. Unfortunately, Nowak and Yuen did not discuss the thermocouple-use issue at all, and therefore the reliability question will have to remain forever unanswered.

Other heat-flux targeted experiments have been performed in more recent years. In Japan, Takizawa et al. [12] and Matsuda et al. [13,14] have been working on the subject matter, although they have provided only temperature measurements. Several Russian experimental activities were reviewed by Bityurin et al. [15]. In 2007, Bobashev et al. [16] performed a rather interesting experiment with nitrogen flowing at $M = 4$ past a sharp-cone/cylinder. The configuration features a pointed electrode at the cone tip and a ring electrode at the cone base; therefore, electric currents can pass between the nitrogen flow and the body. The heat flux was measured in two points of the cylindrical part via bismuth-monocrystal sensors based on the transversal Seebeck effect [17]. Although the data are still being processed and interpreted, the heat flux seems to increase when the electric current is allowed to pass, similar to the results found by Nowak and Yuen [9]. This experiment is very challenging for flow-solver validation, because the correct implementation of the electromagnetic boundary conditions, even for the case of the nonconducting body, are not yet fully mastered, and the boundary conditions for the conducting body introduce a level of complexity that is still beyond computational reach and, perhaps, physical understanding.

In 2002, the aerothermodynamics section of ESA initiated a series of research activities [18–26] motivated by a preliminary collaborative study on the electrodynamic-heat-shield concept, performed by EADS-Astrium in Bremen during the preceding two years. The outcome of the study generated interest in investigating the influence that electromagnetic fields can exert on the heat transfer to a body invested by hypersonic flows; in this regard, spacecraft thermal protection during planetary reentry represented the driving engineering application. The most challenging activity in the

[¶]In what little experimental work was done, apparently nothing surfaced in the literature between the appearance of Ziemer and Bush's [4] (July 1958), Ziemer's [5] (September 1959), and Wilkinson's [6] experiments (1964); curiously enough, Wilkinson did not mention Ziemer and Bush's [5] work at all.

collection is undoubtedly the one [19–23] that aims at the development of numerical algorithms to couple thermochemical-disequilibrium hypersonic-flow-governing equations and Maxwell equations governing the electromagnetic field; in this context, the word *fully* means that the coupling between the sets of field equations is enforced *without* the widespread assumptions of 1) negligible displacement-current density, 2) negligible electric-charge density, and 3) conduction-current density characterized exclusively by Ohm law. (Readers interested in the theoretical motivations justifying such a choice of enforcing the coupling are referred to [18].) The achievement of the objectives set by this numerical research activity presupposes a successful validation exercise hinged on the accurate prediction of experimentally obtained heat-flux data. In this regard, it was felt that the experiments described in [6,9] did not meet an acceptable level of reliability, mainly because the freestream properties were not completely determined by experimental means. Therefore, another activity was added to the collection mentioned earlier that concentrated on the performance of ground experiments involving several geometrical configurations and aimed, as a main target, at the clean determination of heat-flux and corresponding freestream data with and without the application of an external magnetic-induction field for the purpose of computational-fluid-dynamics (CFD) validation. The results of the experiments should also lead to a better understanding of physical phenomena. The major test campaigns were carried out in the period between December 2007 and January 2008 in the 1.4 MW test leg (L2K) of the arc-heated facility LBK (LichtbogenBeheizter Windkanal Köln) belonging to the Windtunnel Department of the Institute of Aerodynamics and Flow Technology of the DLR, German Aerospace Center in Cologne. This paper reports the evolution of this experimental activity and its very important findings. A validation workshop will be organized in which CFD teams will be invited to numerically rebuild the experimentally investigated flowfields. It will be a *blind* validation exercise in the sense that the heat-flux experimental data will be released in absolute units *only* after the numerical simulations have been performed. Readers are therefore forewarned that the information provided in the following sections is tailored to allow meaningful and unambiguous understanding of the experimentally investigated physical and fluid-dynamics phenomenology but to prevent *premature* numerical simulations.

The exposition of the paper is structured as a logical sequence touching on the necessary steps involved in this experimental work: namely, the description of the experimental tools, model design and verification, characterization of the externally applied magnetic-induction field, characterization of freestream and flow conditions, detailed data analysis, and relative discussion of the experimental results.

II. Experimental Tools

Two blunt-body models with integrated magnet coils were investigated in a hypersonic high-enthalpy ionized-argon flowfield. Argon was chosen mainly for consistency with the research activity [19–23] (see Sec. I) concerned with numerical-algorithm development that takes advantage of the moderately complex thermodynamics, chemical kinetics, and transport-coefficient scheme associated with argon plasmas; congruence with past heat-flux targeted experiments [6,9] constituted an additional motivation.

The flow conditions were chosen in such a way as to provide a sufficient level of ionization in the shock-layer region of the flow, particularly in the vicinity of the stagnation point. Expectedly, the total electromagnetic field (externally applied plus induced) influences the path of ions and free electrons and leads to a change in the topology of the flowfield in such a way that the heat flux to the model's surface is reduced.

The tests were carried out in the L2K facility; its principal component is a Huels-type arc heater with a maximum electrical power of 1.4 MW that allows cold-wall heat fluxes up to 2 MW/m^2 at stagnation pressures up to 15 kPa in airflow. Hypersonic freestream velocities are provided by a convergent–divergent nozzle. The nozzle's expansion part is conical with a half-angle of 12 deg. Throat diameters from 14 to 29 mm are available and can be combined with nozzle-exit diameters of 50, 100, 200, and 300 mm. So the facility setup can effectively be adapted to test-campaign-particular necessities. A more detailed description is given by Gülhan et al. [27–29].

The externally applied magnetic-induction field was produced by a direct electric current circulating in a coil. The intensity of the magnetic-induction field could be varied by adjusting the electric-current intensity. The power supply was able to provide intensities up to 2000 A at a voltage level of 18 V and with a ripple of less than 1%. The electric connections between the power supply and coil were realized by tubes of electrolytic copper and were electrically isolated with nonconducting heat shrink tubes. A special feed through the test-chamber walls was manufactured to let the tubes reach the coil. A special glue was used for sealing the passage. A flexible copper cable was installed inside the test chamber to allow mechanical positioning of the test model, which was installed on a two-axis traversing system. The copper liner used for the coil was attached to these flexible cables. During experiments, electric-current intensity and voltage of the power supply and actual model position were continuously recorded by the LBK data-acquisition system.

A. Test Model and Design Verification

Two different test configurations, referred to as C2 and C3, were tested. The C2 model is a hemispherical cylinder, and the C3 model has the same cylindrical geometry but with a flat front surface (Fig. 1). In addition to the definition of the models' outer shape, the magnetic-induction field in the stagnation-point region was another design parameter. Two main aspects had to be considered:

1) The models' interior had to provide enough space to house the coil, including mechanical, electrical, and cooling-related connectors.

2) The model dimensions had to not exceed the limits that cause hypersonic-flow blockage.

A compromise had to be found between these conflicting requirements. Smaller models avoid flow blockage. Larger models make it easier to integrate a powerful coil that, in turn, produces a more intense magnetic-induction field and to remove the heat generated by the electric current in the coil. The surface material of the models was specified to be electrically nonconductive with a negligible polarization and magnetization. Additionally, a material with a sufficiently high melting point was required, because the model's surface is exposed to high thermal loads in high-enthalpy flows. Quartz is known to meet these requirements, although its dielectric constant is between 4.5 and 5; its applicability at surface temperatures as high as 1200 K, its low thermal conductivity, and its negligible electrical conductivity were the reasons for our choice.

The C2 model consists of a cylinder with a hemispherical cap at its end (Fig. 1). The cylinder is oriented along the flow axis with the hemisphere facing the flow. The coil axis was specified to be coincident with the cylinder axis to achieve coincident geometrical and electromagnetic axial symmetry. The design of the coil was driven by maximizing the magnetic-induction field in the stagnation-point area, with allowance to accommodate permanent magnets (if necessary). An insulation material (alumina) was placed between the cylinder front wall and yoke material [Vacoflux 50 (see [30])] to avoid heat transfer to or from the interior part of the model. The C3 model does not have the hemispherical cap and offers a flat surface to the flow, but it can also accommodate permanent magnets.

The design of the magnets was supported with the two-dimensional finite-element-method magnetics calculations using commercial software [31]. To reduce the problem's complexity, only magnetically relevant parts of the setup (i.e., the core and the copper windings) were included in the simulation. The windings were simulated as a single block.

To check the model and coil design and to avoid malfunctions during testing, several characterization and verification tests were performed. The electrical conductivity of the quartz glass was checked at room temperature and at a temperature higher than 250°C. The electrical resistance was measured to be greater than 20 GΩ at

both temperatures. Another approach was used to measure the temperature dependence of the dielectric constant of the quartz material. A quartz cylinder was first heated in an oven and then inserted into a cylindrical capacitor. The capacitor's total capacity was measured while the quartz was cooling down; no change of the capacity was observed. The aerothermal stability of the model was checked by performing stagnation-point tests on the quartz material. A steady-state maximum surface temperature of 960°C, measured by a pyrometer, settled in and no anomalies were observed on the quartz material during and after the test.

The model setup was installed in the test chamber and the electric circuitry was tested under a no-flow condition to demonstrate safe operation. The tests were performed under atmospheric conditions for different coil currents. All sensors integrated in the model were connected to the data-acquisition system to demonstrate their correct integration and the correct operation of the data-acquisition system. Even under real test conditions at low test-chamber pressures, no significant difficulties were experienced because a good electrical insulation of the experimental setup was easily accomplished due to the large dimensions of the L2K test chamber.

Preliminary tests with the C2 model were performed to check for any electric-current leakage through the coil and for the performance of the cooling-water and electric-current supply. After that, magnetic-induction measurements were carried out. The intensity of the field was measured by a magnetometer at specified locations and for different electric currents in the coil. Measurements were taken for both configurations. Measured magnetic field distributions around the C2 model along the axial and radial directions are plotted in Fig. 2. The radial distance (r direction) is measured relative to the cylinder axis. The axial distance (x direction) is measured relative to the stagnation point with an estimated accuracy of ± 0.5 mm.

The intensity of the magnetic-induction field decreases rapidly along the axial distance from the model surface. The influence of the electric current in the coil on the field becomes weaker at high currents because of saturation effects in the yoke. The radial profiles at three different positions on the model axis show a rapid decrease of the field with increasing distance along the model's centerline. The axial distribution is similar (Fig. 3) for the C3 model, but the radial profile has a broader core and the high-field area affects a larger part of the model surface. As expected, the maxima of the field profile on the model surface are located at the sharp edges of the model.

B. Measurement Techniques

Gas mass-flow rate, reservoir, pitot pressure, arc current, arc voltage, and electric-current intensity in model coils were continuously measured and monitored during each test. In addition to these sensor-based measurements, the following quantities were obtained by nonintrusive measurement techniques: 1) gas composition (in particular, ionization level) by emission spectroscopy, 2) freestream velocity and translational temperature by diode laser absorption spectroscopy (DLAS), 3) rotational temperature of nitric-oxide molecules (seeded in argon flow) by laser-induced fluorescence (LIF), 4) free-electron number density by microwave

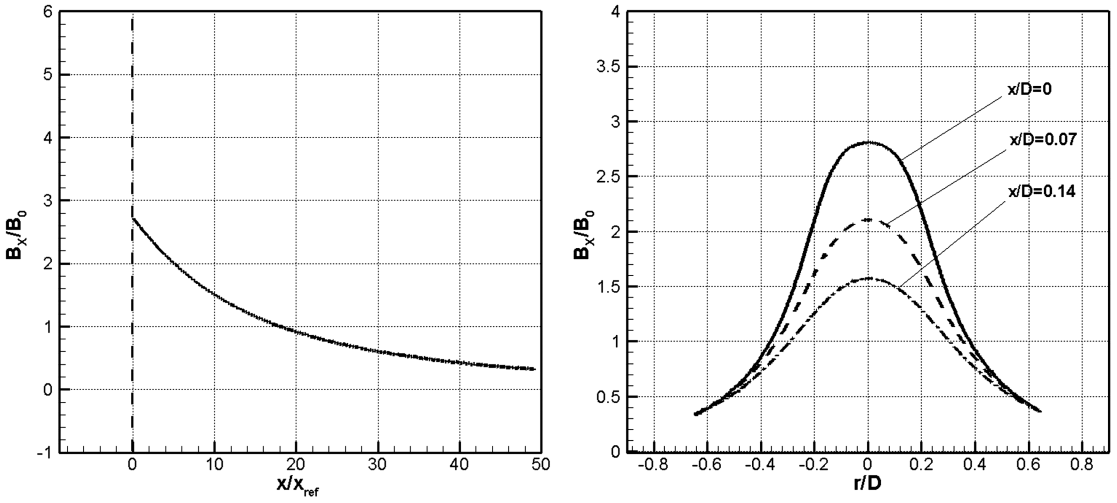

Fig. 2 Measured axial and radial profiles of the magnetic-induction axial component B_x for the C2 model at a coil current of 1000 A.

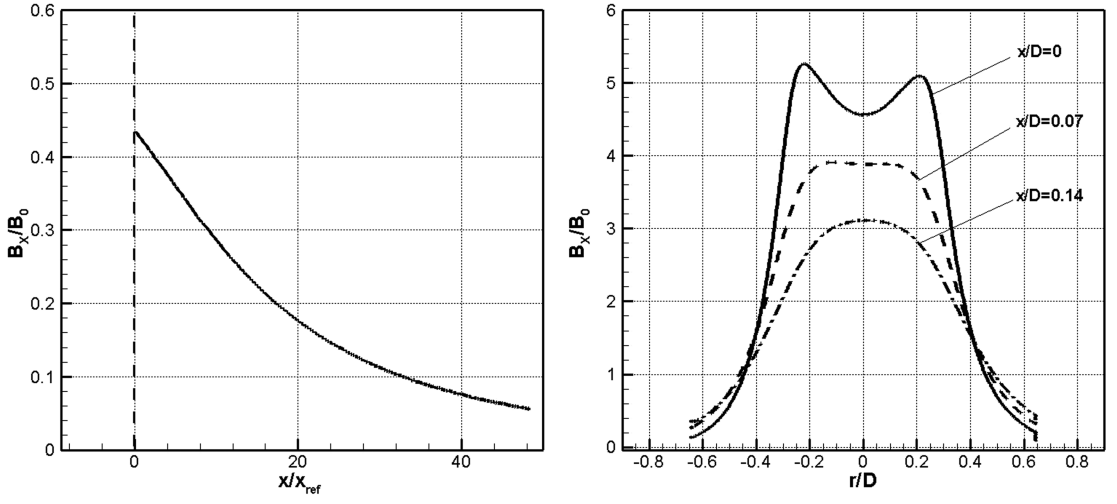

Fig. 3 Measured axial and radial profiles of the magnetic-induction axial component B_x for the C3 model at a coil current of 1000 A.

interferometry, 5) free-electron translational temperature by Langmuir probe, 6) model external-surface-temperature distribution by infrared thermography, 7) surface temperature at the stagnation point by pyrometers, and 8) bow-shock shape and standoff distance by video recording and photography.

Data were sampled at a frequency of 10 Hz and stored electronically. Highly resolved digital photographs and video recordings were taken for each test to allow static and continuous observation of the flow topology. A more detailed description of spectroscopic measurement techniques listed earlier is given in [32–34].

III. Test Procedure and Flow Parameters

During arc-heater ignition, the model was placed outside of the flowfield. When the desired steady-state flow conditions were reached, the model was moved onto the flowfield centerline and the measurements were started. Usually, the coil current was set to the desired level before moving the model into the flow; however, a few dynamic tests were carried out in which the coil current was increased/decreased when the model was already positioned in the flow. At the end of each test, the model was taken out of the flow and then the facility was shut down.

The main flow parameters of the tests are listed in Table 1. Gas mass-flow rate and reservoir pressure were controlled continuously and measured with a precision better than 1%. The other reservoir conditions listed in the table were determined using the former parameters and the nozzle geometry by means of a quasi-one-dimensional flow solver that takes into account high-temperature chemistry [35].

IV. Experimental Results

Numerous tests were carried out to characterize the freestream conditions. DLAS was applied on carbon-monoxide molecules for measuring the flow velocity using a diode laser emitting in the wavelength range from 2330 to 2335 nm at room temperature. DLAS is a line-of-sight method and the interpretation of the measurements has to take into account the homogeneity of the flowfield. The velocity of the gas molecules is proportional to the spectral shift of the absorption signal, and the translational temperature is determined from the half-width of the absorption profile. To provide the required carbon monoxide for DLAS measurements, the argon flow was seeded with 20% of carbon dioxide, which partially dissociates to carbon monoxide at high temperatures. The measurements of the velocity and temperature radial profiles are shown in Fig. 4. DLAS provides a freestream velocity of about 2350 m/s in the flow core region. The measured velocity did not change significantly when the amount of seeding was changed from 5 to 40%. For the measurement conditions in L2K, the divergence of the flow direction tends to increase the extracted velocity value, whereas shear-layer effects in the outer region of the freestream tend to decrease it. As no quantitative information about the divergence of the flow vectors and the thickness of the shear layer is available, the presented data should be used for a qualitative interpretation of the flow properties. The radial decrease in velocity is due to the shear-layer effects in the outer region of the freestream.

The carbon-monoxide translational temperatures shown in the diagram were calculated from the measured half-widths of the absorption signal due to the carbon-monoxide molecules in the flow. It should be kept in mind that DLAS is a line-of-sight technique and that the flow is not parallel. The presence of side regions in which the flow speed drops from its maximum value to zero leads to a broadening of the measured half-widths. This effect increases the measured temperatures, especially when regions far from the center of the flow are considered. For a given velocity, the measured spectral shift is dependent on the angle between the flow direction and the measurement path. Thus, an additional broadening effect appears when the flow is divergent.

Table 1 Flow parameters in the reservoir

Parameters	Values
Gas mass flow rate, kg/s	0.020 ± 0.0002
Reservoir pressure, kPa	37.5 ± 0.75
Specific enthalpy, MJ/kg	2.02 ± 0.12
Total temperature, K	3886 ± 224

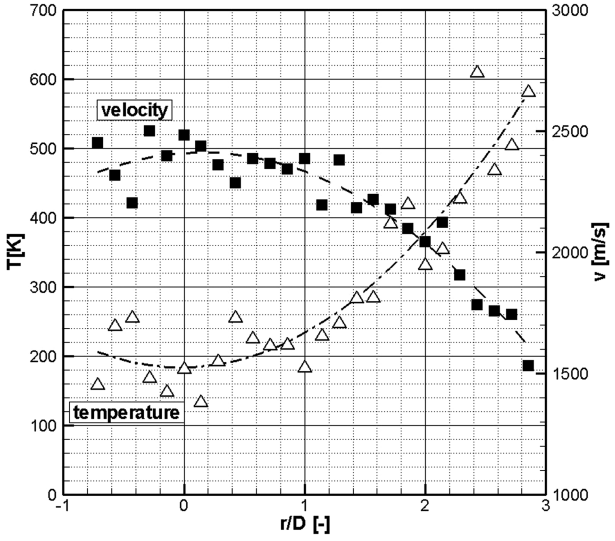

Fig. 4 Velocity and translational-temperature profile in the freestream measured with DLAS: measured values (symbols) and interpolated curve (dashed lines).

For an alternative determination with good spatial resolution of the freestream translational temperature, measurements were also carried out with LIF. About 1% of the nitric oxide was seeded into the argon flow. The temperature was determined from the intensity ratio of fluorescence light from different excited rotational levels under the assumptions that the Boltzmann distribution prevails and that translational and rotational degrees of freedom are in thermal equilibrium so that their temperatures are equal. For sensitivity analysis, measurements were taken for different mass fractions of nitric oxide (Fig. 5). The high spatial resolution of LIF allows measuring the temperature profile from the stagnation point up to the shear layer. Its influence on the freestream translational temperature is relatively small. The reason for the small peak on the axis could not be identified. The average freestream temperature is about 80 K. Behind the bow shock of the C3 model, temperatures close to 3600 K were measured.

Concerning flow visualization, the light emitted from argon-excited atoms or ions provides detailed information of the flowfield (Fig. 6). The top/bottom photographs show the flow pattern when the externally applied magnetic-induction field is turned off/on. The left photographs show a panoramic view of the flowfield; the right photographs illustrate an enlarged view of the shock layer. The bow shock is clearly visible. The appearance of the flowfield changes significantly when the magnetic-induction field is applied. In addition to the marked color change of the flow ahead of and behind the shock, a bright green spot in the stagnation-point region is clearly visible. In contrast to flight circumstances in which ionization takes place behind the bow shock, the freestream was ionized and affected by the electromagnetic field during these experiments. The influence of the electromagnetic field on the shock was quite small; indeed, the shock standoff distance does not seem to be altered and only a slight change in shock curvature is perceptible in the vicinity of the centerline.

To understand the physical process leading to the remarkable change of the flow illumination, emission spectroscopy was applied in both the freestream and shock regions. Spectral peaks in the freestream flow show the presence of argon atoms and ions (Fig. 7, left). Almost all lines in the spectral range from 350 to 690 nm vanish when the magnetic-induction field is applied. Only a small intensity change is noticed for the spectral range from 690 to 900 nm, in which the emission is dominated by argon atoms. It seems that the field

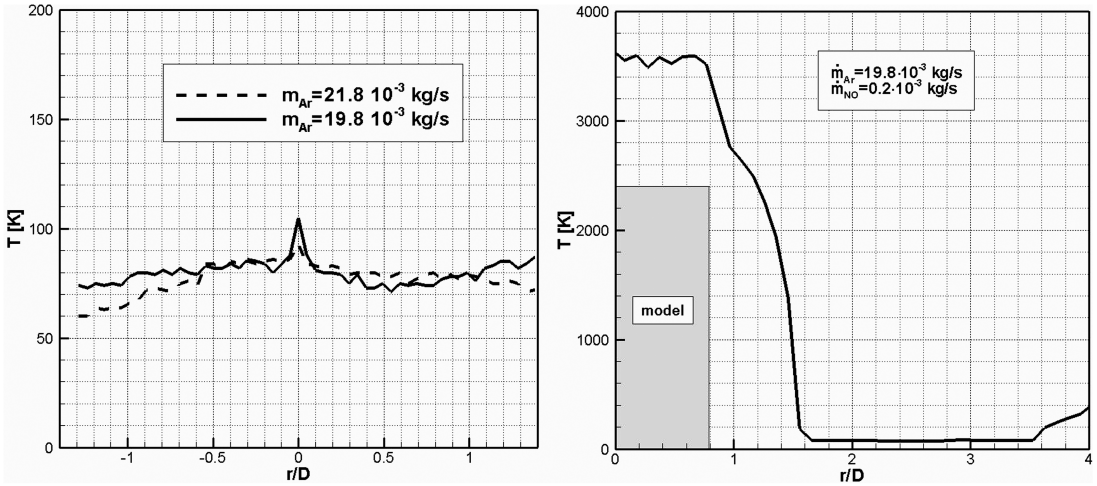

Fig. 5 Measured nitric-oxide rotational temperature in the freestream and around the C3 model.

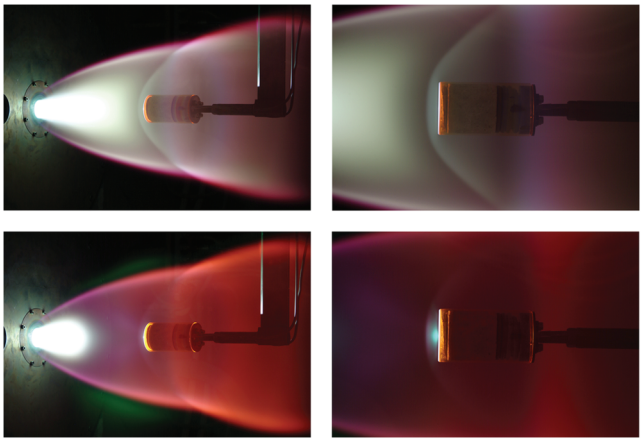

Fig. 6 Photographs of the C3 model during tests without (top) and with (bottom) magnetic-induction field (right photographs show enlarged view of the shock layer).

either pushes those atoms away or deexcites them. The change of the flow illumination to a red color (Fig. 6, bottom) when the magnetic-induction field is on was also observed by Kranc et al. [8] (Sec. 5.7, page 69). According to this team, the red emission of the argon flow is due to excitation of metastable argon atoms with energies of 11.5 and 11.7 eV above the ground state. Collisions of these atoms with electrons induce upward transitions to the lines with large transition probabilities, which are dominant in the red spectral region. When the magnetic field is switched on, the electron temperature rises in the dark space (a broad region ahead of the electron-compression region), due to the high thermal conductivity of the electron gas. The elevated temperature causes a decrease in recombination with the result of lower line radiation from the plasma. The situation behind the shock is different (Fig. 7, right): some of the spectral lines are intensified and appear in good correlation with the bright spot in the stagnation-point region.

Microwave interferometry was used for the measurement of the free-electron number density. This technique measures the microwave phase shift due to changes in the free-electron number density along the measurement line. At selected flow conditions, an average electron density level of 2.8×10^{17} m^{-3} was measured along a measurement beam with a diameter of 80 mm (Fig. 8). In parallel, a Langmuir probe was used primarily for the determination of the free-electron translational temperature and the qualitative number-density history. The output signal of the Langmuir probe is also shown in Fig. 8. Both signals have similar time histories and responses to changes of static pressure. The Langmuir probe was also used to measure the free-electron translational temperature. The right plot in Fig. 8 shows a characteristic curve measured by the probe; each dot represents a measurement point. The curve shows a linear behavior for currents up to 50 mA; at greater currents, there is a transition to saturation. The free-electron translational temperature is estimated from this transition point and the slope of the characteristic curve. The estimated electron temperature is about 6500 K$\pm$ 1500 K.

The models' external-surface-temperature distribution was measured with an infrared (IR) camera and two pyrometers (spectral and two-color). The IR camera has a spectral range of 8–12 μm. The pyrometer data are more accurate than the IR data because of their narrow spectral range (reduced uncertainty with respect to emission-coefficient setting). Therefore, the IR measurements were calibrated by using pyrometer-measured temperatures. Figure 9 shows the IR images of the C2 model during tests with and without a magnetic-induction field. The effect of the field on the surface-temperature distribution is clearly visible near the stagnation point. The temperature at the stagnation point of the C3 model decreases significantly (about a factor of 3) when the field is applied (Fig. 10). The size of the cooled region is strongly correlated to the bright spot observed in front of the model (Fig. 6).

A thermal analysis of the quartz body was performed to determine the heat-flux rate from the measured surface-temperature history by solving the one-dimensional heat-transfer equation. Initial conditions and temperature evolution on the front surface were known from the infrared measurements [36,37]. The boundary condition on the rear surface was defined by the alumina insulation disc placed between the quartz surface and the yoke material to minimize the heat transfer and to set a well-defined boundary condition for the heat-transfer equation (Fig. 11). Several calibration experiments were carried out for the definition of the rear-surface boundary condition by measuring the front- and rear-surface temperatures. Because the integration of thermocouples inside the model would be incompatible with the presence of the magnetic-induction field, calibration tests were carried out without the field. Several thermocouples measured the rear-surface-temperature history of the isolator material (T_2 in Fig. 11). From these data, a coefficient for the heat transfer between the isolator's rear surface and the model's interior parts was deduced. It was assumed that this coefficient remains valid in the presence of the magnetic-induction field. Finally, the heat-flux rate was calculated using the measured front-surface-temperature history, the rear-surface heat-transfer coefficient, and the material parameters of the model. The method allows computing convective, conductive, and radiative heat fluxes at the surface. The convective heat flux is the sum of the conductive heat flux transferred into the model and the radiative heat flux that is emitted to the environment according to the Stefan–Boltzmann relation.

Figure 12 shows the measured surface temperature and the computed heat-flux history for the C2 model with and without a

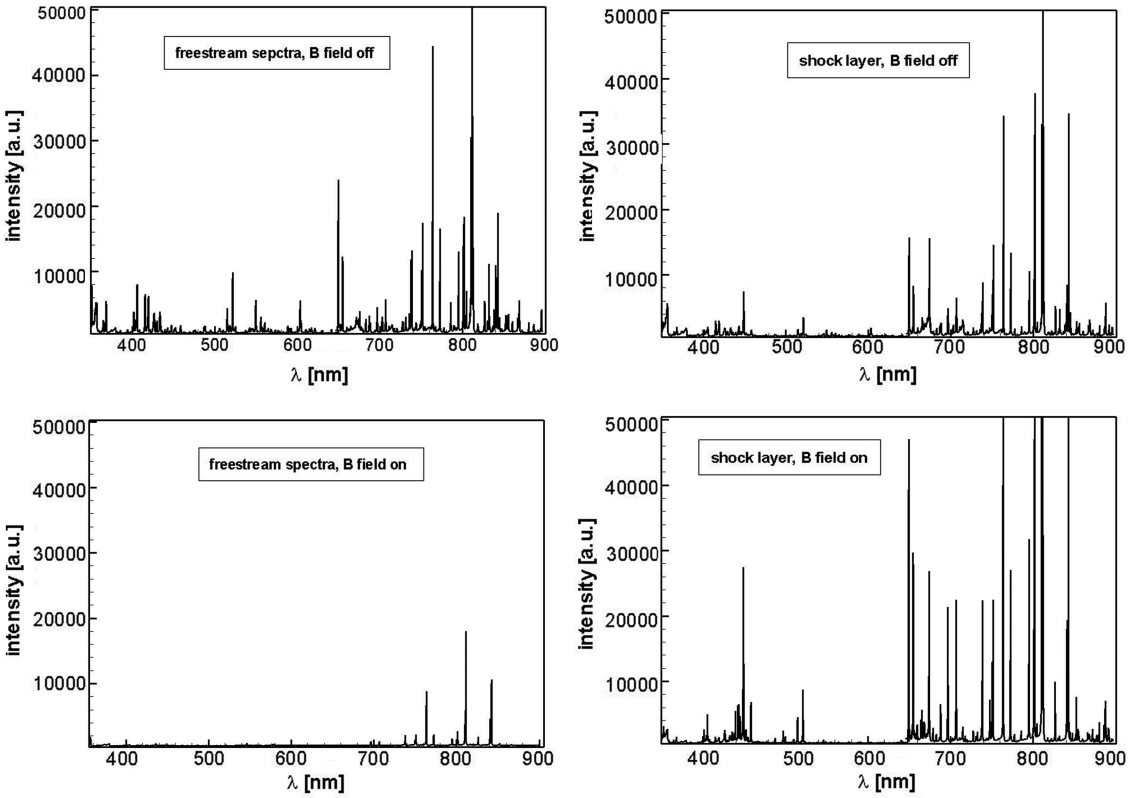

Fig. 7 Measured emission spectra in the freestream (left) and in the shock layer (right) of the C3 model.

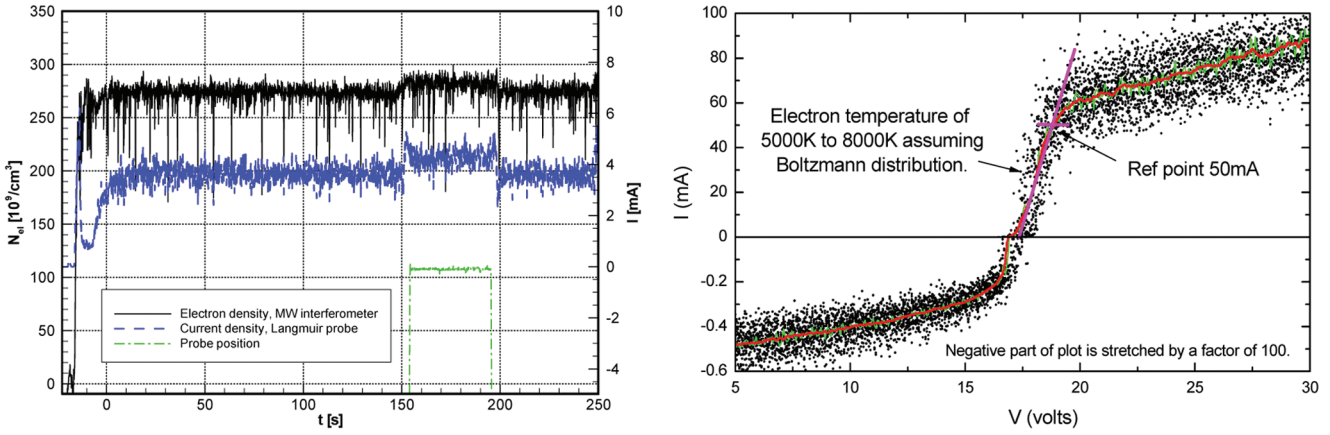

Fig. 8 Measured freestream free-electron number density and translational temperature with microwave interferometer and Langmuir probe.

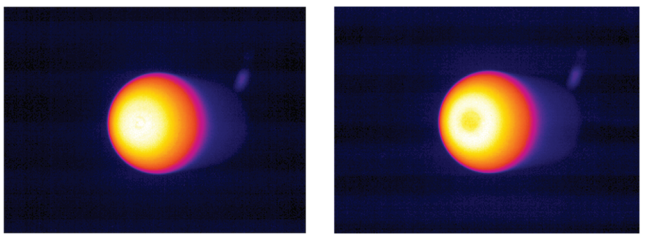

Fig. 9 IR images of the C2 model without (left) and with (right) applied magnetic-induction field.

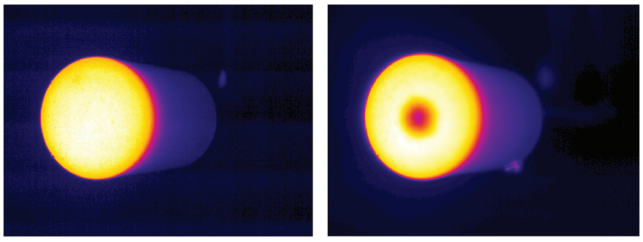

Fig. 10 IR images of the C3 model without (left) and with (right) applied magnetic-induction field.

magnetic-induction field. The left diagram includes the conductive part of the heat flux only. As mentioned before, the model was kept outside the flow until steady-state flow conditions were achieved. In the case without a field, the surface temperature gradually increases, as expected, to a certain level. An increasing surface temperature causes higher radiative heat loss from the model surface to the cooled test-chamber walls. In consequence, the conductive heat flux decreases with time. The sum of the two heat-flux contributions represents the total heat flux and is shown in the right diagram of Fig. 12. For the case with a field, the latter was switched on and

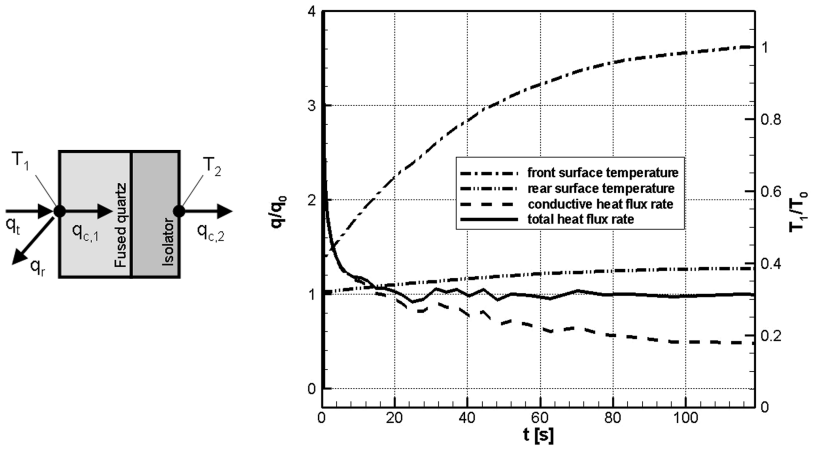

Fig. 11 Calibration test to verify heat-flux determination from temperature measurements.

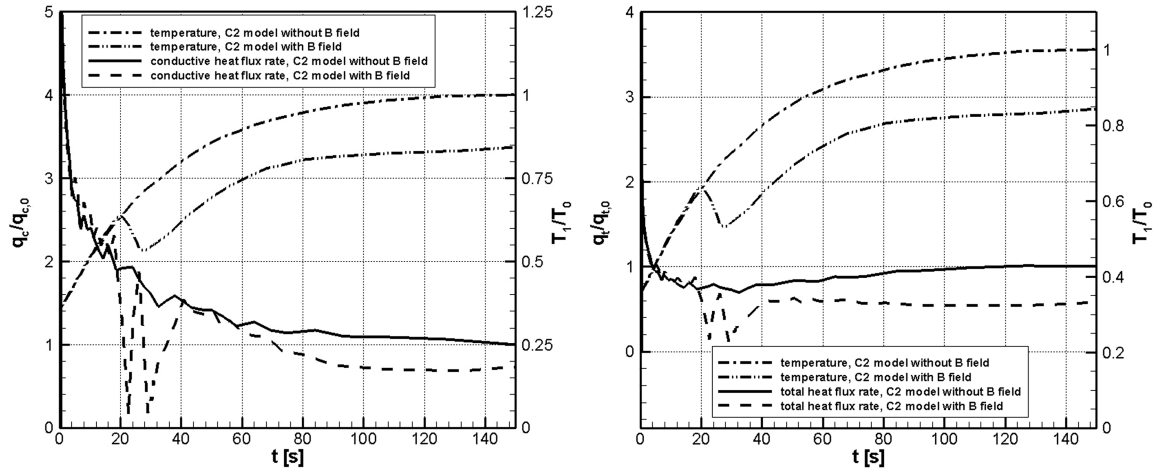

Fig. 12 Comparison of measured surface temperature and heat-flux rate evolution of the C2 model with and without magnetic-induction field.

increased to its steady-state value before the model was brought into the flow. For yet-to-be-explained reasons, it takes about 20 s after model placement in the flow until the magnetic-induction field starts to influence the heating of the model. This phenomenon was also observed during all repetition tests. The surface temperature decreases 16% with respect to the situation without a field. This translates to a reduction of about 35% for the conductive heating: a relevant result with a view to thermal protection. The decrease in total heat flux is 46%.

The electromagnetic effect on the flat-faced C3 model are more pronounced. As shown in Fig. 13, the magnetic-induction field leads to a significant 44% decrease of the surface temperature. This results in a more than 73% reduction of the conductive heating and a drastic 85% mitigation of the total heat flux: a remarkable outcome when compared with previously reported [6,9] experimental results. In contrast to what happened for the C2 model, there was no temporal delay: the electromagnetic field affected the surface temperature and heat-flux rate right from the beginning.

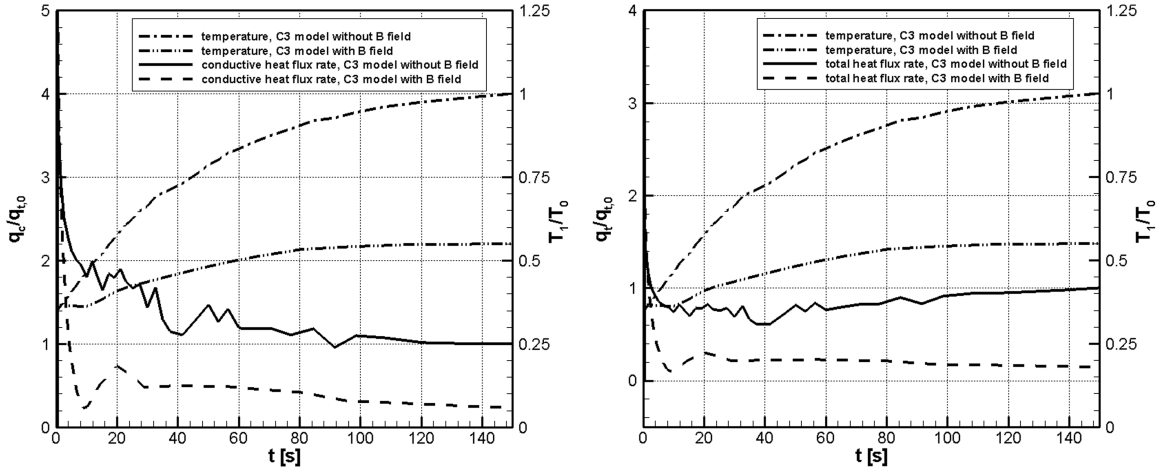

Fig. 13 Comparison of measured surface temperature and heat-flux rate evolution of the C3 model with and without magnetic-induction field.

V. Conclusions

In the frame of this study, dedicated experiments were carried out on heat-flux mitigation by electromagnetic fields on two cylindrical models, one with a hemispherical nose and one with a flat face, in a partially-ionized-argon flow. Tests were carried out in the DLR arc-heated facility L2K in Cologne. The electromagnetic field was generated by coils implemented in the models. The design of models and coils was driven by the requirements of a controllable externally applied magnetic-induction field and prevention of influences due to electrical conductivity, polarization, and magnetization of the materials used in the interior of the model. The freestream conditions of the partially-ionized-argon flow were characterized by applying sophisticated nonintrusive measurement techniques. The main results of this experimental study conducted with ionized-argon flows are undoubtedly represented by the remarkable measured surface-temperature reductions (16% for the C2 model and 44% for the C3 model) and correspondingly derived heat-flux mitigation (46% for the C2 model and 85% for the C3 model) that turned out to occur in the presence of an externally applied magnetic-induction field with respect to the circumstance of field absence. The less pronounced mitigation effect for the C2 model is obviously explained by the lower level of magnetic-induction intensity realized in the stagnation-point region as a consequence of the limited yoke material in the nose region of the model due to geometrical restrictions. Our results confirm the potential benefits derived from the application of electromagnetic fields on hypersonic flows, for aerospace applications in general, and more particularly, in terms of heat-flux mitigation for the purpose of spacecraft thermal protection during atmospheric (re)entry brought to the attention of the aerothermodynamics community by Resler and Sears [1,2]. From a qualitative point of view, our experimental findings in terms of heat-flux reduction agree with those of Wilkinson [6] and contrast the slight heat-flux increase measured by Nowak and Yuen [9] for the case of an electrically nonconducting body. The novelty of our experimental approach with respect to previous heat-flux targeted experiments resides in the following:

1) Adequacy of the model design has been achieved with respect to its scaling to freestream dimensions and choice of appropriate materials.

2) Greater accuracy of the measured data has been achieved due to the use of infrared thermography as the main measurement technique, unaffected by operational difficulties arising from the existence of an electromagnetic environment.

3) Strenuous efforts have been invested in the quantitative characterization of the freestream conditions.

There are, of course, several issues left open to detailed investigations and understanding. Flow characterization in the freestream was carried out in the absence of the externally applied magnetic-induction field and has to be completed; although this aspect is of particular relevance for the planned validation workshop mentioned in Sec. I, we believe its completion does not constitute a reason for delaying communication of the experimental results achieved so far. The accuracy of the free-electron translational-temperature measurement has to be improved. The applicability of measurement techniques in electromagnetic environments has to be investigated and possibly adapted. The study of the impact on the flow pattern of the coil electric-current polarity is very important not only from an experimental point of view, but also to assess the limits of validity of simplified computational models based on the magnetic-induction equation. Finally, investigations of the influence of the electromagnetic field on pressure distributions and aerodynamic forces and moments is another area with plenty of work awaiting to be carried out. Progress along these avenues of research is important and highly desirable.

References

[1] Resler, E., and Sears, W., The Prospects for Magneto-Aerodynamics, *Journal of the Aeronautical Sciences*, Vol. 25, Apr. 1958, pp. 235–245/258.

[2] Resler, E., and Sears, W., "The Prospects for Magneto-Aerodynamics —Correction and Addition," *Journal of the Aero/Space Sciences*, Vol. 26, No. 5, May 1959, pp. 318.

[3] Sears, W., "Magnetohydrodynamic Effects in Aerodynamic Flows," *ARS Journal*, June 1959, pp. 397–406.

[4] Ziemer, R., and Bush, W., "Magnetic Field Effects on Bow Shock Standoff Distance," *Physical Review Letters*, Vol. 1, No. 2, July 1958, pp. 58–59. doi:10.1103/PhysRevLett.1.58

[5] Ziemer, R., "Experimental Investigation in Magneto-Aerodynamics," *ARS Journal*, Sept. 1959, pp. 642–647.

[6] Wilkinson, J., "Magnetohydrodynamic Effects on Stagnation-Point Heat Transfer from Partially Ionized Nonequilibrium Gases in Supersonic Flow," *Proceedings of the 3rd Symposium on Engineering Aspects of Magnetohydrodynamics*, edited by N. Malher, and G. Sutton, Gordon and Breach, New York, 1964, pp. 413–438.

[7] Cambel, A. B., Yuen, M. C., Porter, R., Nowak, R., Kranc, S., and Chang, C., "Theoretical and Experimental Studies of Magneto-Aerodynamic Drag and Shock Standoff Distance," NASA CR-70315, 1966.

[8] Kranc, S., Yuen, M. C., and Cambel, A. B., "Experimental Investigation of Magnetoaerodynamic Flow around Blunt Bodies," NASA NASA CR-1393, 1969.

[9] Nowak, R., and Yuen, M., "Heat Transfer to a Hemispherical Body in a Supersonic Argon Plasma," *AIAA Journal*, Vol. 11, No. 11, Nov. 1973, pp. 1463–1464. doi:10.2514/3.50611

[10] Lees, L., "Laminar Heat Transfer over Blunt-Nosed Bodies at Hypersonic Flight Speeds," *Jet Propulsion*, Vol. 26, No. 4, Apr. 1956, pp. 259–269.

[11] Fay, J. A., and Riddell, F. R., "Theory of Stagnation Point Heat Transfer in Dissociated Air," *Journal of the Aeronautical Sciences*, Vol. 25, No. 2, Feb. 1958, pp. 73–85.

[12] Takizawa, Y., Sato, S., Abe, T., and Konigorski, D., "Electro-Magnetic Effect on Shock Layer Structure in Reentry-Related High-Enthalpy Flow," 35th Plasmadynamics and Lasers Conference, AIAA Paper 2004-2162, Portland, OR, 2004.

[13] Matsuda, A., Wakatsuki, K., Takizawa, Y., Kawamura, M., Otsu, H., Konigorski, D., Sato, S., and Abe, T., "Shock Layer Enhancement by Electro-Magnetic Effect for Spherically Blunt Body," 37th Plasmadynamics and Lasers Conference, AIAA Paper 2006-3573, San Francisco, June 2006.

[14] Matsuda, A., Kawamura, M., Takizawa, Y., Otsu, H., Konigorski, D., Sato, S., and Abe, T., "Experimental Investigation of the Hall Effect for the Interaction between the Weakly-Ionized Plasma Flow and Magnetic Body," 45th Aerospace Sciences Meeting and Exhibit, AIAA Paper 2007-1437, Reno, NV, Jan. 2007.

[15] Bityurin, V., Bocharov, A., and Lineberry, J., "MHD Flow Control in Hypersonic Flight," 13th International Space Planes and Hypersonic Systems Technologies, AIAA Paper 2005-3225, Capua, Italy, May 2005.

[16] Bobashev, S., Golovachov, Y., Chernyshev, A., Mende, N., Sakharov, V., Schmidt, A., and Wie, D. M. V., "Magnetohydrodynamic Influence on Supersonic Gas Flows: Experimental Modeling and Numerical Simulation," *Journal of Propulsion and Power* (submitted for publication).

[17] Bobashev S., Mende, N., Sakharov, V., Sopozhnikov, S., Mityakov, V., Mityakov, A., and Wie, D. M. V., "Application of Gradient Heat Flux Sensor in Shock Tube Experiments," 43rd Aerospace Sciences Meeting and Exhibit, AIAA, Paper 2005-787, Reno, NV, Jan. 2005.

[18] Giordano, D., "Hypersonic-Flow Governing Equations with Electromagnetic Fields," 33rd Plasmadynamics and Lasers Conference, AIAA Paper 2002-2165, Maui, HI, May 2002.

[19] D'Ambrosio, D., and Giordano, D., "Electromagnetic Fluid Dynamics for Aerospace Applications. Part 1: Classification and Critical Review of Physical Models," 35th AIAA Plasmadynamics and Lasers Conference, AIAA Paper 2004-2165, Portland, OR, 2004.

[20] D'Ambrosio, D., Pandolfi, M., and Giordano, D., "Electromagnetic Fluid Dynamics for Aerospace Applications. Part 2: Numerical Simulations Using Different Physical Models," 35th AIAA Plasmadynamics and Lasers Conference, AIAA Paper 2004-2362, Portland, OR, 2004.

[21] D'Ambrosio, D., and Giordano, D., "A Numerical Method for Two-Dimensional Hypersonic Fully Coupled Electromagnetic Fluid Dynamics," 36th AIAA Plasmadynamics and Lasers Conference, AIAA, Paper 2004-5374, Toronto, June 2005.

[22] D'Ambrosio, D., and Pandolfi, M., "An Upwind Numerical Method for the Prediction of Ideal MHD High Speed Flows," 35th Plasmadynamics and Lasers Conference, AIAA Paper 2004-2164, Portland, OR, 2004.

[23] D'Ambrosio, D., and Giordano, D., "Electromagnetic Fluid Dynamics for Aerospace Applications," *Journal of Thermophysics and Heat Transfer*, Vol. 21, No. 2, Apr.–June 2007, pp. 284–302. doi:10.2514/1.24732

[24] Bruno, D., Laricchiuta, A., Capitelli, M., Catalfamo, C., Chikhaoui, A., Kustova, E., and Giordano, D., "Transport Properties of Equilibrium Argon Plasma in a Magnetic Field," 35th Plasmadynamics and Lasers Conference, AIAA Paper 2004-2161, Portland, OR, 2004.

[25] Bruno, D., Catalfamo, C., Laricchiuta, A., Giordano, D., and Capitelli, M., "Convergence of Chapman-Enskog Calculation of Transport Coefficients of Magnetized Argon Plasma," *Physics of Plasmas*, Vol. 13, No. 072307, 2006, pp. 1–7. doi:10.1063/1.2221675

[26] Bruno, D., Laricchiuta, A., Capitelli, M., Catalfamo, C., and Giordano, D., "Transport Properties of Partially Ionized Argon in a Magnetic Field," Plasmadynamics and Lasers Conference, AIAA Paper 2007-4137, Miami FL, June 2007.

[27] Gülhan, A., and Esser,B., "Arc-Heated Facilities as a Tool to Study Aerothermodynamic Problems of Reentry Vehicles," *Advanced Hypersonic Test Facilities*, edited by F. K. Lu, D. E. Marren, Progress in Astronautics and Aeronautics, Vol. 198, AIAA, Reston, VA, 2002, pp. 375–403.

[28] Gülhan, A., and Esser, B., "A Study on Heat Flux Measurements in High Enthalpy Flows," 35th AIAA Thermophysics Conference, AIAA Paper 2001-3011, Anaheim, CA, June 2001.

[29] Gülhan, A., Esser, B., Koch, U., and Hannemann, K., "Mars Entry Simulation in the Arc Heated Facility L2K," *Proceedings of the 4th European Symposium on Aerothermodynamics for Space Vehicles*, ESA-SP-487ESA Publications Div., Noordwijk, The Netherlands, Feb. 2002, pp. 665–772.

[30] "Weichmagnetische Kobalt-Eisen-Legierungen," Vacuumschmelze GmbH & Co. KG, Rept. PHT-004, Hanau, Germany, 2001.

[31] Meeker, D., "Finite Element Method MagneticsVersion 4.0, User's Manual," 2004, http://femm.foster-miller.net/Archives/doc/manual.pdf.

[32] Del Vecchio, A., Palumbo, G., Koch, U., and Gülhan, A., "Temperature Measurements by Laser-induced Fluorescence Spectroscopy in Nonequilibrium High Enthalpy Flow," *Journal of Thermophysics and Heat Transfer*, Vol. 14, No. 2, Apr.–June 2000, pp. 216–224.

[33] Grisch, F., Bouchardy, P., Joly, V., Koch, U., and Gülhan, A., "Coherent Anti-Stokes Raman Scattering Measurements and Computational Modeling of Nonequilibrium Flow," *AIAA Journal*, Vol. 38, No. 9, Sept. 2000, pp. 1669–1675. doi:10.2514/2.1152

[34] Koch, U., Esser, B., and Gülhan, A., "Two Dimensional Spatially Resolved Two Photon Oxygen Atom Laser Induced Fluorescence Measurements in the Flow Field of the Arc Heated Facility L3K," *Proceedings of the 5th European Symposium on Aerothermodynamics for Space Vehicles*, ESA-SP-563ESA Publications Div., Noordwijk, The Netherlands, Feb. 2005, pp. 493–500.

[35] Bade, W. L., and Yos, J. M., "The NATA Code, Theory and Analysis," NASA CR-2547, 1975.

[36] Henckels, A., and Gruhn, P., "Study on Aerothermal Effects of Viscous Shock Interaction in Hypersonic Inlets," *Proceedings of the 5th European Symposium on Aerothermodynamics for Space Vehicles*, ESA-SP-563ESA Publications Div., Noordwijk, The Netherlands, Feb. 2005, pp. 553–558.

[37] Häberle, J., and Gülhan, A., "Internal Flowfield Investigation of a Hypersonic Inlet at Mach 6 with Bleed," *Journal of Propulsion and Power*, Vol. 23, No. 5, Sept.–Oct. 2007, pp. 1007–1017. doi:10.2514/1.29669

I. Boyd
Associate Editor